Impact of Supercritical Fluid Solvent Quality on Polymer Conformation in Semidilute Solutions: SANS Data for Poly(ethylene-*co*-1-butene) in Dimethyl Ether to Kilobar Pressures

T. P. DiNoia,[†] J. H. van Zanten,[*,‡] S. R. Kline,[#] Alberto Garach-Domech,[^] M. A. McHugh,[*,#] P. J. Wright,[⊥] and L. J. Fetters[§]

Department of Chemical Engineering, Johns Hopkins University, Baltimore, Maryland 21218; Chemical Engineering Department, North Carolina State University, Box 7905, Raleigh, North Carolina 27695-7905; Department of Chemical and Biomolecular Engineering, Cornell University, Ithaca, New York 14853; ExxonMobil Research and Engineering Co., Annandale, New Jersey 08801; NIST, Center for Neutron Research, 100 Bureau Drive, Stop 8562, Gaithersburg, Maryland 20899; and Department of Chemical Engineering, Virginia Commonwealth University, Richmond, Virginia 23284

Received May 23, 2003; Revised Manuscript Received July 29, 2003

ABSTRACT: Phase behavior and small-angle neutron scattering (SANS) measurements are reported for poly(ethylene-*co*-20.2 mol % 1-butene) (PEB_{10}) dissolved in supercritical dimethyl ether (DME). The phase boundary is located at pressures near 600 bar at 130 °C, and it exhibits a minimum in temperature near 105 °C where the cloud-point pressure rises sharply. Neutron scattering is performed with a high-pressure scattering cell designed for a large incident beam diameter, good mixing, and real-time viewing of the solution to ensure single-phase operation. The SANS results suggest significant variations in intramolecular correlations exist at length scales proportional to a few monomer units although the radius of gyration remains close to the unperturbed value at pressures from the cloud point to as high as 2400 bar. As expected, the intermolecular correlation length grows rapidly on approach to the phase boundary. The phase behavior and SANS data suggest that DME is very poor quality solvent even at high solvent densities.

Introduction

Although supercritical fluids (SCF) are being used as alternative solvents for processing polymers,[1−9] the state of the art for modeling polymer solubility in an SCF solvent does not allow for reliable a priori predictions of solution behavior.[10−13] The tunable solvent power of a supercritical fluid provides opportunities for innovative processing techniques but also presents a formidable challenge for describing the density dependence of the intermolecular potential functions for highly compressible SCF−polymer solutions. Fortunately, there now exists a sizable database on the solubility of polymers in SCF solvents[13] from which useful heuristics can be gleaned. Large changes in polymer solubility can result from modest changes in polymer architecture since most supercritical fluids are very poor quality solvents relative to liquids even when the SCF solvent is compressed to liquidlike densities.[14] The conditions needed to dissolve a polymer cannot be rationalized solely as a result of SCF density, especially when polymer−polymer, solvent−solvent, or polymer−solvent pairs can exhibit temperature-sensitive interactions, such as complex formation or hydrogen bonding. However, a weak, but tunable, SCF solvent provides an opportunity to explore the response of the solution microstructure to changes in the system temperature, pressure, and density.[14,15] It is more difficult to probe large regions of chemical potential space with changes in pressure and temperature when using an incompressible liquid solvent.

Within the past few years, small-angle neutron scattering (SANS) studies have been used to determine the behavior of a polymer chain at the mixture critical concentration, in the semidilute overlap regime, in SCF, and in liquid solvents.[14−18] These SANS studies report that the radius of gyration (R_g), which is associated with polymer intramolecular correlations, is close to the theta (θ)-melt value as the mixture critical point is approached with changes in pressure or temperature. However, over the same operating space, intermolecular correlations characterized by the correlation length (ξ) rapidly increase near the mixture critical point and can exceed the magnitude of R_g, indicating the presence of strongly interacting unperturbed coils. The observations from these early SANS studies[14−18] agree with the predictions of Muthukumar[19] and Raos and Allegra[20] that polymer chains remain in the unperturbed state as the solvent quality is adjusted below the θ-condition and throughout the poor solvent regime until the critical boundary is reached.

The objective of the present work is to determine the phase behavior of poly(ethylene-*co*-20.2 mol % 1-butene) (PEB_{10}) in dimethyl ether (DME) and to relate those macroscopic observations with solution microstructure information obtained from SANS measurements in the single-phase region of the PEB_{10}−DME phase diagram. This combined phase behavior−SANS study builds on an earlier study reported for PEB_{10} in supercritical ethane (T_c = 32.2 °C, P_c = 48.8 bar) and in liquid pentane (T_c = 196.4 °C, P_c = 33.7 bar).[14] Although DME

[†] Johns Hopkins University.
[‡] North Carolina State University.
[§] Cornell University.
[⊥] ExxonMobil Research and Engineering Co.
[#] NIST, Center for Neutron Research.
[^] Virginia Commonwealth University.
* Corresponding authors. Mark A. McHugh: e-mail mmchugh@vcu.edu; John H. van Zanten: e-mail john_vz@ncsu.edu.

10.1021/ma034690d CCC: $25.00
Published on Web 08/26/2003

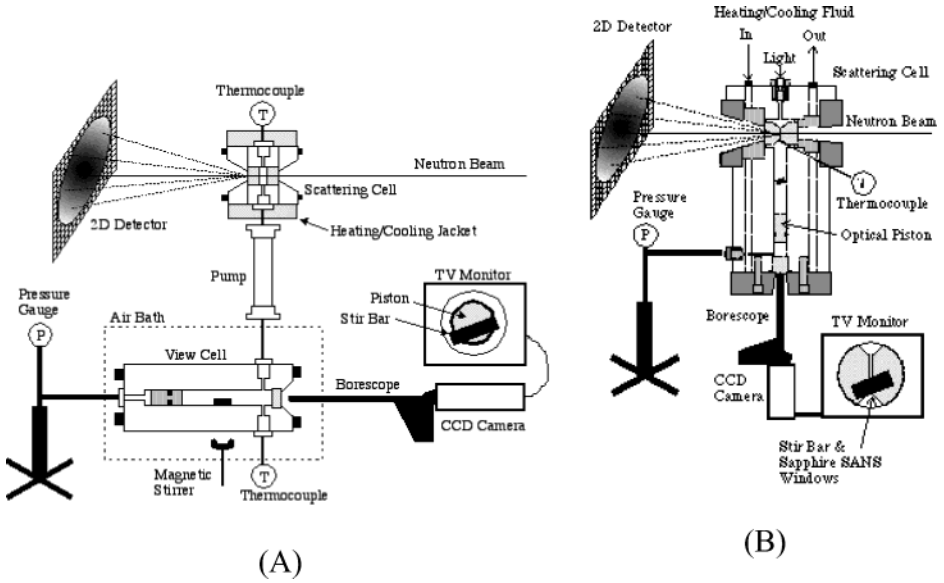

Figure 1. Schematic diagram of the neutron scattering cell and associated equipment used by DiNoia et al.[14] (A) compared to the high-pressure, unibody scattering cell used in the present study (B).

(T_c = 126.8 °C, P_c = 52.4 bar) has a dipole moment of 1.3 D, it can dissolve poly(ethylene) at pressures near 600 bar,[21] and therefore, DME provides an opportunity to probe the same pressure−temperature space with SANS as that probed with nonpolar ethane and pentane. Another objective of the present work is to describe an improved experimental apparatus for SANS measurements of SCF−polymer solutions. In the PEB_{10}−alkane study reported by DiNoia et al.,[14] scattering measurements were made with the two-cell apparatus shown in Figure 1A, consisting of a variable-volume view cell, a transfer pump, and a separate neutron scattering cell. It should be noted that PEB_{10} has a melting temperature near 100 °C so that elevated temperatures are needed for SANS measurements of SCF−PEB_{10} solutions. The two-cell system requires large amounts of expensive deuterated materials to fill both cells and the transfer lines, constant monitoring to maintain equilibrium conditions, special care to maintain leak-free seals on a large number of connections maintained at temperatures in excess of 100 °C, and a significant amount of labor and time to disassemble and clean between experiments. Figure 1B shows an improved apparatus that merges the scattering and view cell into a single, high-pressure "unibody" cell for ease of SANS measurements of solutions at pressures to 2500 bar and temperatures in excess of 130 °C. The design and operation of the unibody cell are described in the following section.

Experimental Section

Materials. DME (99.0% minmum purity) is obtained from Aldrich Chemical Co., and deuterated DME-d_6 (99.8% minimum purity; D, 99%) is obtained from CDN Isotopes. The poly(ethylene-*co*-20.2 mol % 1-butene) (h-PEB_{10} and d-PEB_{10}, respectively) copolymers are synthesized via anionic polymerization of butadiene with subsequent saturation by hydrogenation or deuteration as described in detail elsewhere.[22−25] The h-PEB_{10} and d-PEB_{10} are statiscally random copolymers with approximately 10 ethyl branches per 100 carbon atoms, weight-average molecular weights (M_W) of 232 500 and 232 800, respectively, and molecular weight distributions of 1.01−1.06.

Experimental Apparatus. The phase behavior of the polymer−SCF mixtures are determined prior to SANS experiments from cloud-point measurements using equipment and techniques described in detail elsewhere.[6,26,27] Each cloud point is reproduced two or three times at each temperature with a scatter of approximately ±5.0 bar. Mixture critical points are the temperature, pressure, and polymer concentration where two phases of equal volume are observed at the phase transition, which is also accompanied by reddish-orange opalescence.

Figure 1B shows a schematic diagram of the unibody scattering cell (11.5 cm o.d × 24 cm long) that is constructed from Nitronic 50, a high-nickel-content austenitic steel. To view the solution, one end of the cell is fitted with a sapphire window (1.91 cm o.d. × 1.91 thick to within ±0.003 cm, Hemlite quality, Crystal Systems, MA) rated to 6800 bar based on an unsupported area of 1.27 cm^2 and a safety factor of 10. The window is sealed with an elastomeric O-ring/back-up ring combination in a configuration recommended by Lentz.[28] The cell contents are mixed using a stir bar controlled by a magnet located outside of the cell. The cell contents are projected onto a video monitor using a CCD camera (COHU, Inc.) coupled to a borescope (Lenox Corp.) placed directly against the sapphire window located at one end of the cell. Pressure is transmitted to the solution via an optically clear, floating, quartz piston displaced by the action of a manual, high-pressure generator (HIP Inc., model 37-5.75-60) that delivers optically clear oil (Syltherm XLT, Dow Chemical Corp.) to the backside of the piston. System pressure is measured on the oil side of the piston with a digital pressure transducer (Viatran Corp., model 245, 0−3450 bar, accurate to within ±3.5 bar). A small correction of 1 bar is added to account for the pressure required to displace the piston. The physical state of the polymer−SCF mixture is monitored via the sapphire window-pressurizing fluid−glass piston pathway.

Sapphire windows (2.54 cm o.d. × 1.91 cm thick to within ±0.003 cm, Hemex quality, Crystal Systems, MA) are located near the front of the cell and are positioned to allow the neutron beam to pass radially through the cell. The end of each window that wets the SCF solution is coned to 1.91 cm o.d. on a 45° angle to allow the solution to mix uniformly throughout the cell. The path length between the inner surfaces of the two windows is adjustable between 0.10 and 0.95 cm using window spacers placed between the window and the plug on the beam inlet side of the cell. The bolted plug that secures the window on the beam inlet side of the cell has an 8° included-angle cone, and the bolted plug that secures the window on the detector side has an 18° included-angle cone. Both windows are rated to 3100 bar based on an unsupported area of 2.85 cm^2 and a safety factor of 10. The window and plug configurations allow a neutron beam up to 1.91 cm in

diameter to pass unobstructed through the scattering cell, providing a high neutron flux and a wide range of scattering angles. We have never had a window failure in more than 10 years of experience operating view cells with sapphire windows of similar unsupported area, sealing configuration, and pressure rating. However, on occasion, O-ring failures at high operating temperatures have occurred which result in the rapid discharge of solution from the cell. Hence, quartz glass "shields" (0.317 cm thick) are attached to the cell on the outside of both the beam inlet and the scattering cell windows so that solution suddenly discharged from the cell is deflected from the SANS instrument.

The temperature of the solution inside the cell is measured with a calibrated type-E thermocouple fitted into a port near the scattering windows and connected to a digital multimeter (Omega Instruments, Inc., model DP465, accuracy ±0.03%). The solution temperature is maintained to within ±0.5 °C with a cell band heater (Rama Corp.) and with circulating fluid flowing through four heating/cooling lines machined into the body of the cell. The band heater is controlled with a PID temperature controller (Omega Instruments, model PN7000) connected to a platinum RTD probe (Omega Instruments) also located in a port near the scattering windows. A recirculating bath (Fisher Scientific, model 1016-D) is used to deliver a heat transfer fluid (Syltherm 800, Dow Chemical) to the internal heating/cooling lines.

Experimental Scattering Technique. Neutron scattering experiments are performed with the unibody scattering cell on the NG-3 30 m SANS spectrometer at the National Institute of Standards and Technology (NIST) located in Gaithersburg, MD. Details of the 30 m SANS instrument at NIST are given elsewhere.[29] A neutron wavelength of 5.0 Å ($\Delta\lambda/\lambda = 0.15$) is used with a sample aperture diameter of 0.95 cm. SANS measurements are performed with three different solutions: 3.6 wt % h-PEB_{10} in DME-d_6, 3.3 wt % h-PEB_{10} in DME-d_6, and 3.4 wt % total polymer, h-PEB_{10} + d-PEB_{10}, in DME-d_6. Sample-to-detector distances of 13.55 and 2.55 m are used to obtain overlapping q ranges of 0.006 $Å^{-1} \le q \le 0.04$ $Å^{-1}$ and 0.02 $Å^{-1} \le q \le 0.29$ $Å^{-1}$, respectively where $q = 4\pi/\lambda \sin(\theta/2)$ and θ is the scattering angle.

The measured intensities are corrected for dark-noise background, detector efficiency, scattering from the empty cell with sapphire windows, sample transmission, and sample path length changes that result from window displacement at high pressures as described by DiNoia et al.[14] The scattered intensities are radially averaged and converted to an absolute differential scattering cross section per unit volume, $d\Sigma/d\Omega$ (cm^{-1}), using cross-section calibration standards of silica and water for the low and high q ranges, respectively. Solvent scattering is neglected since fully deuterated DME is used in these experiments. A value for the incoherent background scattering mainly from hydrogen in the polymer is set equal to the floating parameter obtained from a fit of the Ornstein−Zernike (OZ) equation to absolute solution scattering intensities over the entire q range.

$$I(q) = \frac{I(0)}{1 + q^2\xi^2} + I_{q\to\infty}^{BKG} \quad (1)$$

With this approach, $I_{q\to\infty}^{BKG}$ ranges from 0.050 cm^{-1} ± 10% to 0.112 cm^{-1} ± 10% for the (h-PEB_{10} + d-PEB_{10})−DME-d_6 and h-PEB_{10}−DME-d_6 solutions, respectively, which is approximately 1% of the magnitude of scattering intensities at low q. Therefore, any error associated with the use of eq 1 has only a minor influence on the values obtained for ξ and R_g.

The new unibody cell design offers several improvements over the two-cell system. First, the new SANS scattering windows and the bolted plug configurations allow for an increase in the incident beam diameter to 1.91 cm, an increase in accessible scattering angles, and an adjustable path length to 0.95 cm. Therefore, a higher neutron flux on the sample is achieved along with an increase in scattered intensities over a range of q values up to 0.29 $Å^{-1}$. Consequently, data acquisition time at a given pressure, temperature, and concentration is on the order of 10−15 min compared to 45−75 min to obtain the same number of statistically significant detector counts with the two-cell system. Second, the unibody cell has a much smaller working volume, which results in a significant decrease in the amount of deuterated polymer and solvent needed per SANS experiment, and it eliminates the recycle pump used with the two-cell system. Third, the solution between the two SANS scattering windows is efficiently maintained at a fixed temperature with the internal heating/cooling lines and the heating band. The internal heating/cooling lines allow for a rapid reduction in the cell temperature even though the thermal mass of the cell is quite large so that the cell can be comfortably handled to turnover a new solution. Fourth, the fluid between the SANS scattering windows is monitored visually during the scattering experiment to ensure a well-mixed, single-phase solution exists during data collection. This online visual measurement of the scattering solution was not possible in the two-cell configuration.

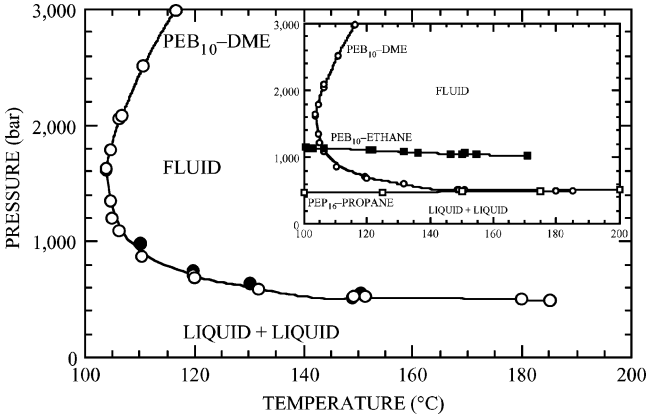

Figure 2. Phase behavior of h-PEB_{10} in DME (open circles) and DME-d_6 (filled circles).[30] The inset plot shows the phase behavior of h-PEB_{10} in DME and in ethane and the phase behavior of the poly(ethylene-*co*-32 mol % propylene) (PEP_{16})−propane system.[33]

Results

Phase Behavior. Figure 2 shows that the cloud-point curve for h-PEB_{10} in DME is at slightly lower pressures than the partial set of data for h-PEB_{10} in DME-d_6,[30] suggesting that DME is a modestly better solvent than DME-d_6. DiNoia et al. have also shown that pentane is a modestly better solvent for h-PEB_{10} than pentane-d_{12}.[14] The slightly higher cloud-point pressures with DME-d_6 are likely due to a decrease in the magnitude of dispersion interactions since the C−D bond length is shorter than the C−H bond length, which reduces the segment volume and the segment polarizability.[31]

Note that the PEB_{10}−DME cloud-point curve exhibits a rapid increase in pressure at temperatures near 105 °C, and in fact, the curve exhibits a positive slope at very high pressures. The type of phase behavior shown in Figure 2 is typical of that found for SCF−polymer mixtures where the SCF solvent is polar and the polymer is nonpolar or vice versa.[13] The interchange energy, ω, shown in eq 2, is expected to be dominated by dipolar DME-DME interactions relative to DME−PEB_{10} cross interactions which leads to the temperature minimum in the cloud-point curve and to the formation of two phases at lower temperatures.

$$\omega = z\left[\Gamma_{DME-PEB_{10}}(r,T) - \frac{1}{2}(\Gamma_{DME-DME}(r,T) + \Gamma_{PEB_{10}-PEB_{10}}(r,T))\right] \quad (2)$$

where z is the coordination number, or the number of solvent−segment pairs, in the SCF−polymer solution.[32] The difference in the solution behavior of a polar−nonpolar mixture to that of a nonpolar−nonpolar mixture is apparent in the inset plot in Figure 2 which compares the PEB_{10}−DME and the PEB_{10}−ethane systems to the poly(ethylene-*co*-32 mol % propylene) (PEP_{16})−propane system.[33] PEP_{16} is also a 1,2 addition, statistically random, nonpolar copolymer with 16 methyl side groups per 100 carbon atoms.[33] Both the PEB_{10}−ethane and PEP_{16}−propane cloud-point curves are relatively flat at temperatures from 100 to ∼200 °C and pressures of 1110 and 500 bar, respectively, which is characteristic of polymer−SCF solvent phase behavior dominated by dispersion interactions. The PEB_{10}−DME and PEP_{16}−propane cloud-point curves essentially superpose at temperatures greater than ∼135 °C where dispersion interactions, which scale as polarizability per molar volume, should be the dominant type of intermolecular interaction in operation. Although the polarizability of DME, 5.2 Å^3, is slightly lower than that of propane, 6.3 Å^3, the molar density of DME is approximately 8% greater than that of propane which means that the polarizability/molar volume is close to the same value for both SCF solvents at the cloud-point pressure at 135 °C. From a macroscopic point of view, DME is a better solvent than ethane for PEB_{10} at high temperatures, but at temperatures near 100 °C, DME rapidly becomes a poor quality solvent as it begins to exhibit more polar character. SANS measurements for the PEB_{10}−DME system are performed at 130 °C for direct comparison to previously published scattering data for PEB_{10} in supercritical ethane and liquid pentane.[14] SANS measurements for the PEB_{10}−DME system are also performed at 110 °C upon approach to the "low"-pressure phase boundary at 870 bar and on approach to the "high"-pressure phase boundary at 2500 bar.

Small-Angle Neutron Scattering. Polymer solution microstructure is determined by SANS using the high-concentration, isotopic labeling technique.[14,16,34,35] The coherent scattered intensity of an incompressible polymer solution, $I(q)$, is given by the following expression

$$I(q) = Nz^2KS_s(q) + Nz^2LS_t(q) \tag{3}$$

where $S_s(q)$ and $S_t(q)$ are the structure factors of the single chain and total chain scattering, respectively, N is the number of polymer molecules, and z is their degree of polymerization. The two contrast parameters K and L are

$$K = (b_h - b_d)^2 x_h x_d \tag{4}$$

$$L = \left(b_h x_h + b_d x_d - \left(\frac{v_p}{v_s}\right) b_s\right)^2 \tag{5}$$

where b is the scattering length, subscripts h and d represent protonated and deuterated polymer repeat groups, respectively, subscript s denotes solvent, x_h and x_d are the mole fractions of protonated and deuterated chains on a solvent-free basis, and (v_p/v_s) is the ratio of the specific volumes of polymer repeat units (v_p in cm^3/monomer) to that of solvent molecules (v_s in cm^3/molecule). Elemental scattering lengths[36] are used to calculate $b_{h-PEB10}$, -0.20×10^{-12} cm, $b_{d-PEB10}$, 4.8×10^{-12} cm, and b_{DME-d_6}, 5.9×10^{-12} cm. The polymer solution concentrations are all very close to the mixture critical concentration. $S_t(q)$ is determined by measuring the scattering from a solution containing only h-PEB_{10} where x_h equals one. The contrast parameter L is calculated for both the 3.3 and 3.6 wt % h-PEB_{10} solutions although this small difference in h-PEB_{10} concentration is not expected to have a discernible effect on the observed scattered intensities. The single chain structure factor, $S_s(q)$, is obtained from solution scattering data with x_h and x_d chosen so that the contrast variation parameter L equals zero, thereby eliminating the total chain scattering contribution. At 110 °C x_d is 0.615 and at 130 °C x_d is 0.616. However, L is not zero at all pressures in this study since the polymer solution is compressible, which means that the second term in eq 3 must be explicitly accounted for when determining $S_s(q)$. Fortunately, literature data are available for the densities of the polymer−solvent mixtures and the pure solvents used in this study.[30] The Tait equation is used to estimate the specific volume of PEB_{10} at elevated pressures.[37] Ideally, the single parameter in the Tait equation is fit to experimental data; however, in this instance, this parameter is estimated as the average of the values reported for branched and linear poly(ethylene)s. Ambient pressure data at 23 and 140 °C[25,38] are used to estimate the specific volume of PEB_{10} at the temperature of interest needed for the Tait equation.

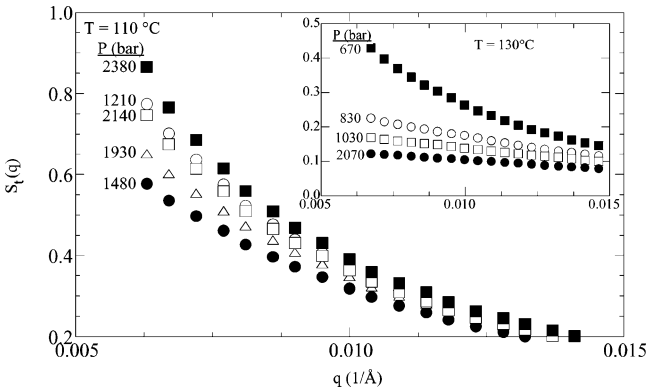

Figure 3. Variation of $S_t(q)$ as a function of pressure at 110 °C and 3.3 wt % h-PEB_{10} and 130 °C and 3.6 wt % h-PEB_{10} (inset plot). The pressure is shown next to each symbol at each temperature. Phase boundaries are located at approximately 900 and 2425 bar at 110 °C and 600 bar at 130 °C. Not all of the pressures are shown to avoid cluttering the plots.

Total solution scattering data are fit to the Ornstein−Zernike (OZ) equation to determine the dependence of the correlation length, ξ, on temperature and pressure.

$$S_t(q) = \frac{S(0)}{1 + q^2\xi^2} \tag{6}$$

At 130 °C the total chain scattering, $S_t(q)$, decreases with increasing pressure over the low q range of data for 3.6 wt % h-PEB_{10} in DME-d_6 (see inset plot in Figure 3) in a manner similar to that previously observed with h-PEB_{10} in SCF alkanes.[14] However, Figure 3 shows that at 110 °C $S_t(q)$ varies nonmonotonically as the pressure increases. This nonmonotonic variation corresponds to the existence of two separate phase boundaries shown explicitly in Figure 2 at low and high pressures at 110 °C. The increase of $S(0)$ and ξ near a phase boundary is readily apparent from these data.

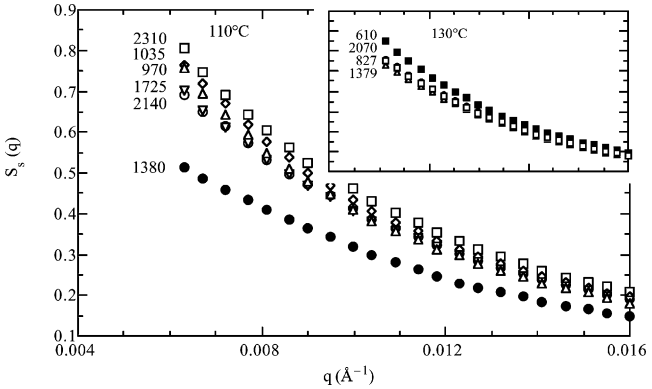

Figure 4. Variation of $S_s(q)$ as a function of pressure at 110 and 130 °C (inset plot with same axes values). Phase boundaries are located at approximately 900 and 2425 bar at 110 °C and 600 bar at 130 °C. At 110 °C: open squares, 2310 bar; open diamonds, 1035 bar; open triangles, 970 bar; inverted open triangles, 1725 bar; open circles, 2140 bar; filled circles, 1380 bar. At 130 °C: filled squares, 610 bar; open circles (partially hidden), 2070 bar; open squares, 827 bar; open triangles, 1379 bar. Not all of the pressures are shown to avoid cluttering the plots.

When $S_s(q)$ is determined, the residual contribution of the total scattering to the apparent single chain scattering is explicitly calculated. L is close to zero for $x_d \sim 0.6$ at 130 and 110 °C at pressures very close to the respective phase boundaries at low pressures. However, L is not identically zero at all pressures since the compressibilities of PEB_{10} and DME-d_6 are not the same as is evident from the change in concentration as a function of solution density. For example, over the operating pressure ranges, the polymer volume fractions, $\phi_p \sim c_p v_p$, change from $0.029 \leq \phi_p \leq 0.032$ for 3.4 wt % h-PEB_{10} in DME-d_6 at 110 °C and from $0.026 \leq \phi_p \leq 0.029$ for the same solution at 130 °C.

Figure 4 shows that there is very little variation in $S_s(q)$ data at 130 and at 110 °C, with the exception of the data at 110 °C and 1380 bar although it is not obvious why this data set differs so much from the other $S_s(q)$ data. Also not shown in Figure 4 are artificially low $S_s(q)$ data at 110 °C and three different pressures. These low scattering data are likely due to the slow rate of dissolution observed for PEB_{10} in DME upon reentry into the one-phase region after crossing into the two-phase region. The solution becomes optically clear, with mixing, almost immediately when the pressure is increased 1000 bar greater than the pressure at the phase boundary. However, even at this elevated pressure well into the single-phase region, it takes approximately 2 h with mixing for the scattering intensity to recover to previously observed values. This lag time occurs as polymer-rich droplets that appear near the phase boundary redissolve into the weak, SCF solvent-rich phase. Unfortunately, this lengthy dissolution time was not noted until well into the SANS study. Hence, artificially low $S_s(q)$ data are rejected from further analysis if obtained following a data set acquired at a pressure very close to the phase boundary. There is no obvious reason to reject the $S_s(q)$ data at 110 °C and 1380 bar since these data were obtained after mixing fresh solution at conditions for 2 h. The Debye equation is used to interpret the $S_s(q)$ data in the low-q limit:

$$S_S(q) = \frac{2}{q^4 R_g^4}[\exp(-q^2 R_g^2) + q^2 R_g^2 - 1] \qquad (7)$$

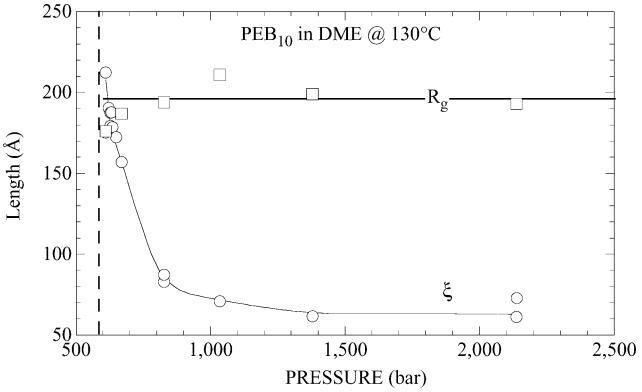

Figure 5. Variation of R_g (open squares) and ξ (open circles) for the PEB_{10}−DME-d_6 system as a function of pressure at 130 °C. The dashed line represents the location of the 130 °C phase boundary at approximately 600 bar.

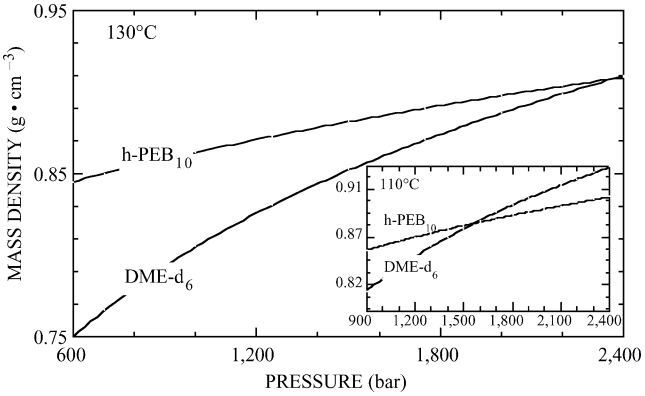

Figure 6. Variation of the mass density of PEB_{10} and DME-d_6[30] as a function of pressure and temperature.

The single chain scattering functions in Figure 4 indicate that there is very little variation in R_g over the pressure range investigated for both temperatures with the exception of the data at 110 °C and 1380 bar.

Figure 5 shows the variation of R_g and ξ as the h-PEB_{10}−DME-d_6 phase boundary is approached isothermally at 130 °C. The R_g values at each pressure are in close agreement with the unperturbed θ-melt value of $R_g = 205$ Å for PEB_{10} as calculated from a previously reported relationship,[25] $R_{g-\theta,melt} \sim 0.42 M_w^{0.5}$. The trend observed in R_g as a function of pressure is similar to the trends reported for PEB−alkane solutions[14] and for polystyrene in liquid cyclohexane and in liquid acetone.[15−17] At distances far from the phase boundary ξ is essentially independent of pressure at a value of 65 Å. However, as expected, ξ dramatically increases near the phase boundary and approaches the magnitude of R_g, behavior similar to that reported for other systems.[14,17,18] Note that the values of ξ near the phase boundary never exceed the value of R_g despite repeated attempts to observe this behavior. This may be indicative of rapid phase separation driven by a relatively large density difference between the polymer-rich and the SCF-rich phases which is not encountered with conventional liquid solvents. Figure 6 shows that the density difference between PEB_{10} and DME at 130 °C is largest at pressures very close to the phase boundary. The variation in ξ provides information on the effect of pressure on DME solvent quality. Melnichenko et al. argue that the demarcation between poor and good solvent quality can be quantified as a "θ-pressure",

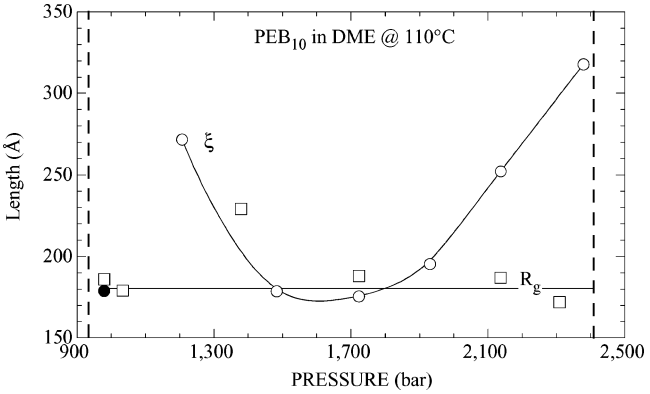

Figure 7. Variation of R_g (open squares) and ξ (open and filled circles) for the PEB_{10}−DME-d_6 system as a function of pressure at 110 °C. The dashed lines represent the locations of the 110 °C phase boundaries at approximately 900 and 2425 bar.

P_θ,[18] using the relationship[39,40]

$$\xi_\theta \sim \frac{R_{g-\theta}}{\sqrt{3}} \tag{8}$$

At 130 °C, ξ_θ equals 118 Å, which corresponds to a P_θ of approximately 750 bar. Hence, the poor solvent regime occurs over a range of ∼150 bar near the phase boundary.

Figure 7 shows R_g and ξ as a function of pressure for h-PEB_{10} in DME-d_6 at 110 °C. The R_g values are again insensitive to pressure although now R_g is ∼170 Å, which is 25 Å lower than that observed at 130 °C. At 110 °C, R_g exhibits similar trends on approach to the phase boundary as observed for other polymer−solvent systems.[14,17,18] Figure 7 shows that ξ exhibits a nonomonotonic variation with pressure, which corroborates the observation that phase boundaries exist for this solution at ∼900 and 2425 bar (see Figure 2). At the low-pressure boundary the determination of ξ is problematic, owing to the weak solvent quality of supercritical DME and to the density difference between the SCF-rich and the polymer-rich domains, as shown in the inset plot in Figure 6. As the boundary is approached the solution becomes slightly hazy as high molecular weight PEB_{10} oligomers begin to precipitate as polymer-rich domains that quickly settle out of the scattering volume. Hence, a significant decrease is observed in the scattering intensity that manifests itself as an underestimated value of ξ as shown by the filled circle in Figure 7. The determination of ξ at the high-pressure boundary is more reliable since the solvent quality of DME is improved and the density of DME is now higher and also slightly greater than the density of PEB_{10}, as seen in the inset plot in Figure 6. Hence, it is possible to operate closer to the high-pressure boundary while still maintaining the single-phase integrity of the solution. At approximately 1610 bar, ξ exhibits a minimum value of 175 Å, which is ∼110 Å greater than the values observed for the same solution at 130 °C and similar pressures and is greater than ξ_θ calculated from eq 8. It is noteworthy that the minimum in ξ also occurs at essentially the same pressure as the minimum in the cloud-point temperature shown in Figure 2. Hence, regardless of the pressure, DME is a poor quality solvent over the entire single-phase region at 110 °C due to the close proximity to the phase boundary at slightly lower temperatures. Melnichenko and co-workers report that at certain temperatures the PDMS−CO_2 system also exhibits a minimum in ξ due to the existence of two separate phase boundaries.[18]

Muthukumar[19] and Raos and Allegra[20] argue that polymer chains in a semidilute solution remain in the unperturbed state as the solvent quality is adjusted below the θ-condition and throughout the poor solvent regime until the phase boundary is reached. The SANS studies performed here, as well as those by Melnichenko and co-workers[15−18] and DiNoia and co-workers,[14] agree with these predictions. The following equation is used to calculate the overlap concentration, c^*, which denotes the onset of the semidilute region

$$c^* = \frac{3M_w}{4\pi N_A R_g^{\,3}} \tag{9}$$

where N_A is Avogadro's number.[39] For the PEB_{10}−DME system with $R_g = R_{g\theta-melt}$, c^* is equal to 1.3 wt %, which suggests that the polymer concentrations used in this study are greater than the overlap concentration, thus justifying the applicability of the theories of Muthukumar[19] and Raos and Allegra.[20]

Conclusions

A new unibody cell design is described for SANS studies of high-pressure polymer−SCF mixtures. A higher neutron flux on the sample is achieved along with an increase in scattered intensities over a range of q values up to 0.29 $Å^{-1}$ so that data acquisition times at a given pressure, temperature, and concentration have been reduced significantly. The unibody cell has a much smaller working volume, which results in a significant decrease in the amount of deuterated polymer and solvent needed per experimental run. A new glass piston design provides a means of visually monitoring the fluid between the SANS scattering windows to ensure that a well-mixed, single-phase solution exists during data collection.

The PEB_{10}−DME system exhibits phase behavior typical of that found for SCF−polymer mixtures where the SCF solvent is polar and the polymer is nonpolar or vice versa.[13] The PEB_{10}−DME cloud-point curve exhibits a rapid increase in pressure at temperatures near 105 °C, and the curve exhibits a positive slope at very high pressures. The interchange energy is expected to be dominated by dipolar DME−DME interactions relative to DME−PEB_{10} cross interactions which leads to the temperature minimum in the cloud-point curve and to the formation of two phases at lower temperatures. Hence, two cloud-point pressures are observed at 110 °C, while a single low-pressure phase boundary is observed at 130 °C. SANS measurements of the static correlation length indicate that the solvent quality at 110 °C is always relatively poor in comparison with that observed for at 130 °C. That is, even under the best of conditions, the 110 °C solution supports concentration fluctuations whose length scale is nearly a factor of 3 larger than those observed for the 130 °C solution. This increase in correlation length at 110 °C is likely due to the close proximity of the phase boundary regardless of the system pressure. In addition, the reported R_g values for PEB10 in DME also agree with the predictions of Muthukumar[19] and Raos and Allegra[20] that polymer chains in a semidilute solution remain in the unperturbed state as the solvent quality is adjusted

below the θ-condition and throughout the poor solvent regime until the phase boundary is reached.

Acknowledgment. The authors acknowledge the National Science Foundation (NSF) for partial support of this project under Grants CTS-9729720 and GER-9454136. This material is based upon activities supported by NSF under Agreement DMR-9986442. This work was also supported in part by the Kenan Center for the Utilization of Carbon Dioxide in Manufacturing. In addition, the authors thank Dr. Ozge Guney, David Rock, Joseph Russell, and Gulu Sandhu at VCU and Shaun Tanner, Chris Kloxin, and Samuil Amin at NC State University for assistance with the SANS experiments. The authors are especially indebted to Mike Franckowiac and Walt Krug, master instrument makers at Johns Hopkins University, for assistance with the design and manufacturing of the high-pressure view and scattering cells used in these studies. Certain trade names and company products are identified to adequately specify the experimental procedure. In no case does such an identification imply recommendation or endorsement by NIST, nor does it imply that the products are necessarily best for the purpose.

References and Notes

(1) Berens, A. R.; Huvard, G. S. In *Supercritical Fluid Science and Technology*; ACS Symposium Series 406; Johnston, K. P., Penninger, J. M. L., Eds.; American Chemical Society: Washington, DC, 1989; Vol. 406, p 207.
(2) Gallagher, P. M.; Coffey, M. P.; Krukonis, V. J.; Klasutis, N. In *Supercritical Fluid Science and Technology*; Johnston, K. P., Penninger, J. M. L., Eds.; American Chemical Society: Washington, DC, 1989; Vol. 406, p 334.
(3) McNally, M. E. P.; Deardorff, C. M.; Fahmy, T. M. In *Supercritical Fluid Technology*; Bright, F. V., McNally, M. E. P., Eds.; American Chemical Society: Washington, DC, 1992; Vol. 488.
(4) Garrabos, Y.; Leneindre, B.; Subra, P.; Cansell, F.; Pommier, C. *Ann. Chim. Sci. Mater.* **1992**, *17*, 55.
(5) McHugh, M. A.; Krukonis, V. J. *Supercritical Fluid Extraction, Principles and Practice*, 2nd ed.; Butterworth-Heinemann: Boston, 1994.
(6) DeSimone, J. M.; Maury, E. E.; Menceloglu, Y. Z.; McClain, J. B.; Romack, T. J.; Combes, J. R. *Science* **1994**, *265*, 356.
(7) Canelas, D. A.; Betts, D. E.; DeSimone, J. M. *Macromolecules* **1996**, *29*, 2818.
(8) Cooper, A. I.; Hems, W. P.; Holmes, B. H. *Macromol. Rapid Commun.* **1998**, *19*, 353.
(9) Poliakoff, M.; Darr, J. A. *Chem. Rev.* **1999**, *99*, 495.
(10) Hasch, B. M.; McHugh, M. A. *J. Polym. Sci., Part B: Polym. Phys. Ed.* **1995**, *33*, 715.
(11) Lee, S. H.; Hasch, B. M.; McHugh, M. A. *Fluid Phase Equilib.* **1996**, *117*, 61.
(12) Hasch, B. M.; Lee, S. H.; McHugh, M. A. *J. Appl. Polym. Sci.* **1996**, *59*, 1107.
(13) Kirby, C. F.; McHugh, M. A. *Chem. Rev.* **1999**, *99*, 565.
(14) DiNoia, T. P.; Kirby, C. F.; van Zanten, J. H.; McHugh, M. A. *Macromolecules* **2000**, *33*, 6321.
(15) Melnichenko, Y. B.; Anisimov, M. A.; Povodyrev, A. A.; Wignall, G. D.; Sengers, J. V.; Van Hook, W. A. *Phys. Rev. Lett.* **1997**, *79*, 5266.
(16) Melnichenko, Y. B.; Wignall, G. D. *Phys. Rev. Lett.* **1997**, *78*, 686.
(17) Melnichenko, Y. B.; Wignall, G. D.; Van Hook, W. A.; Szydlowski, J.; Wilczura, H.; Rebelo, L. P. *Macromolecules* **1998**, *31*, 8436.
(18) Melnichenko, Y. B.; Kiran, E.; Wignall, G. D.; Heath, K. D.; Salaniwal, S.; Cochran, H. D.; Stamm, M. *Macromolecules* **1999**, *32*, 5344.
(19) Muthukumar, M. *J. Chem. Phys.* **1986**, *85*, 4722.
(20) Raos, G.; Allegra, G. *J. Chem. Phys.* **1996**, *104*, 1626.
(21) Lee, S. H.; LoStracco, M. A.; Hasch, B. M.; McHugh, M. A. *J. Phys. Chem.* **1994**, *98*, 4055.
(22) Rachapudy, H.; Smith, G. G.; Raju, V. R.; Graessley, W. W. *J. Polym. Sci., Part B: Polym. Phys. Ed.* **1979**, *17*, 1211.
(23) Kirgas, T. M.; Carella, J. M.; Struglinski, M. J.; Crist, B.; Graessley, W. W. *J. Polym. Sci., Part B: Polym. Phys.* **1985**, *23*, 509.
(24) Balsara, N. P.; Fetters, L. J.; Hadjichristidis, N.; Lohse, D. J.; Han, C. C.; Graessley, W. W.; Krishnamoorti, R. *Macromolecules* **1992**, *25*, 6137.
(25) Fetters, L. J.; Graessley, W. W.; Krishnamoorti, R.; Lohse, D. J. *Macromolecules* **1997**, *30*, 4973.
(26) Meilchen, M. A.; Hasch, B. M.; McHugh, M. A. *Macromolecules* **1991**, *24*, 4874.
(27) Mertdogan, C. A.; Byun, H.-S.; McHugh, M. A.; Tuminello, W. H. *Macromolecules* **1996**, *29*, 6548.
(28) Lentz, H. *Rev. Sci. Instrum.* **1969**, *40*, 371.
(29) Glinka, C. J.; Barker, J. G.; Hammouda, B.; Krueger, S.; Moyer, J. J.; Orts, W. J. *J. Appl. Crystallogr.* **1998**, *31*, 430.
(30) Byun, H. S.; DiNoia, T. P.; McHugh, M. A.; Wright, P. S.; Fetters, L. J. *J. Appl. Polym. Sci.*, unpublished data.
(31) Rabinovich, I. B. *Russ. Chem. Rev.* **1962**, *31*, 51.
(32) Prausnitz, J. M.; Lichtenthaler, R. N.; de Azevedo, E. G. *Molecular Thermodynamics of Fluid-Phase Equilibria*, 3rd ed.; Prentice Hall: Englewood Cliffs, NJ, 1999.
(33) Chen, S.-J.; Banaszak, M.; Radosz, M. *Macromolecules* **1995**, *28*, 1812.
(34) Akcasu, A. Z.; Summerfield, G. C.; Jahshan, S. N.; Han, C. C.; Kim, C. Y.; Yu, H. *J. Polym. Sci., Part B: Polym. Phys. Ed.* **1980**, *18*, 863.
(35) King, J. S.; Boyer, W.; Wignall, G. D.; Ullman, R. *Macromolecules* **1985**, *18*, 709.
(36) Sears, V. F. *Neutron News* **1992**, *3*, 26.
(37) Rodgers, P. A. *J. Appl. Polym. Sci.* **1993**, *48*, 1061.
(38) Fetters, L. J.; Lohse, D. J.; Richter, D.; Witten, T. A.; Zirkel, A. *Macromolecules* **1994**, *27*, 4639.
(39) Fujita, H. *Polymer Solutions*; Elsevier Science Publishers B.V.: Amsterdam, 1990.
(40) des Cloizeaux, J.; Jannink, G. *Polymers in Solution: Their Modelling and Structure*; Oxford University Press: Oxford, 1990.

MA034690D